Glass Surface Detection: Leveraging Reflection Dynamics in Flash/No-flash Imagery

Tao Yan*, Hao Huang, Yiwei Lu, Zeyu Wang, Ke Xu, Yinghui Wang, Xiaojun Chang, Rynson W.H. Lau

Abstract—Glass surfaces are ubiquitous in daily life, typically appearing colorless, transparent, and lacking distinctive features. These characteristics make glass surface detection a challenging computer vision task. Existing glass surface detection methods always rely on boundary cues (e.g., window and door frames) or reflection cues to locate glass surfaces, but they fail to fully exploit the intrinsic properties of the glass itself for accurate localization. We observed that in most real-world scenes, the illumination intensity in front of the glass surface differs from that behind it, which results in variations in the reflections visible on the glass surface. Specifically, when standing on the brighter side of the glass and applying a flash towards the darker side, existing reflections on the glass surface tend to disappear. Conversely, while standing on the darker side and applying a flash towards the brighter side, distinct reflections will appear on the glass surface. Based on this phenomenon, we propose NFGlassNet, a novel method for glass surface detection that leverages the reflection dynamics present in flash/no-flash imagery. Specifically, we propose a Reflection Contrast Mining Module (RCMM) for extracting reflections, and a Reflection Guided Attention Module (RGAM) for fusing features from reflection and glass surface for accurate glass surface detection. For learning our network, we also construct a dataset consisting of $\sim 3.3K$ no-flash and flash image pairs captured from various scenes with corresponding ground truth annotations. Extensive experiments demonstrate that our method outperforms the state-of-the-art methods. Our code, model, and dataset will be available upon acceptance of the manuscript.

Index Terms—Glass Surface Detection, no-flash and flash Image Pair, Reflection Detection, Deep Learning.

I. INTRODUCTION

■ LASS surfaces, including glass walls, glass doors, french windows, glass tabletops, and glass railings are prevalent in daily life. Glass surfaces lack distinctive external features and their appearances mainly depend on surroundings, which poses challenges for related computer vision tasks such as autonomous driving and 3D reconstruction. In the past few years, several single visible (RGB) image-based glass surface detection methods [1], [3]-[8] have been proposed and achieved good performance in the daytime. However, most of these methods heavily rely on boundary cues [1], [4], [5], reflection or ghosting cues [3], [7], and moreover, limited cues embedding in a single RGB image may result in detection failures in challenging scenes. Recently, several multi-modal based methods [10], [13], [14], [54], [65] are able to identified glass surfaces with different types of sensors. However, these methods usually require extra expensive sensors in addition to regular cameras, and multi-modal image alignment and fusion.

We can observe a valuable phenomenon that the illumination intensity of the space in front of a glass surface (e.g., glass wall, door, or window) is often different from that of the space behind in daily life. Typically, when we take photographs from

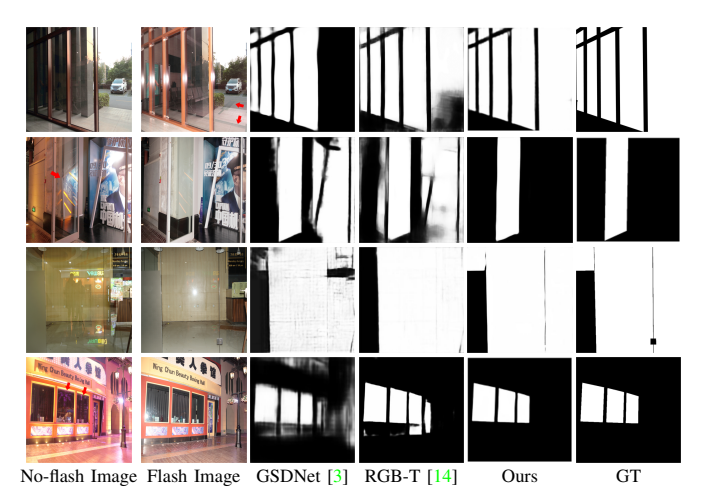
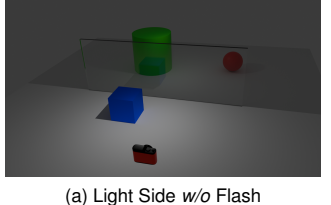
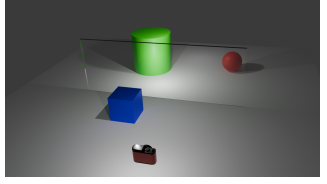


Fig. 1. Comparison of our *NFGlassNet* with the state-of-the-art glass surface detection methods. For each scene from left to right: the first and second columns are no-flash image and flash image, respectively, and the rest columns are results produced by the competing methods and our method. GSDNet [3] tends to a under-detection when there is no reflection on the glass surface (1st scene, no-flash image). Both GSDNet [3] and RGB-T [14] are prone to over-detection when there are numerous glass-like frame (2nd scene), as they heavily rely on the boundary cues. Our method can effectively leverage the appearance and disappearance of reflections in the same scene, which enables more accurate identification of glass regions. The red arrows indicate the locations of reflections, and zooming in on the images can provide a better visual effect.

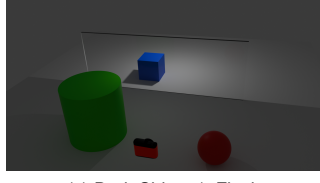
the brighter side of a glass surface towards the other darker side, there are always obvious reflections on the glass surface in the captured image. However, while a flash accompanying the camera toward the glass surface is applied, the reflections tend to be weakened and even disappear, since the dark space behind the glass is also illuminated, as shown in Fig. 1. Conversely, when we photograph from the darker side of the glass, there usually will not appear very obvious reflections on the glass surface, but applying a flash while shooting would result in more prominent reflections on the glass surface.

This observation can be illustrated in Fig. 2, and the camera's views of the observation are further shown in our supplementary material. We rendered these examples with different illumination intensities with Blender [46]. Specifically, Fig. 2a shows that a prominent reflection (blue box) will appear on the glass surface, if the lighting intensity of the space in front of the glass surface is obviously stronger than that of the space behind the glass surface. Fig. 2b shows that while a flash accompanying the camera is applied, the lighting intensity of the darker side behind the glass surface will be enhanced. Then, the reflection appeared on the glass surface will become indistinguishable and even be overshadowed by the transmission layer. Therefore, the no-flash and flash image





(b) Light Side w/ Flash





(c) Dark Side w/o Flash

(d) Dark Side w/ Flash

Fig. 2. Scenes rendering by Blender for appearance (1st scene) and disappearance (2nd scene) of reflection: Distinct reflection on the glass surface will disappear when take photographs from the high-lighted side and apply flash towards the darker side (from Fig. 2a to Fig. 2b). Conversely, in some situations, clear reflection will appear on the glass surface when we take photographs from the low-lighted side and apply flash towards the light side (from Fig. 2c to Fig. 2d).

pair shown in Fig. 2a and 2b is able to aid in reflection cue extraction and glass surface detection. Similarly, in Fig. 2c, the camera in the darker side of the glass surface cannot capture obvious reflection due to insufficient lighting. Then, as shown in Fig. 2d, while a flash is applied, the dark space in front of the glass surface will be illuminated, resulting in prominent reflections on the glass surface. Thus, the no-flash and flashimage pair shown in Fig. 2c and 2d can contribute to glass surface detection.

Several real-world scenes without and with flash are shown in Fig. 1. As shown in the 1st scene, when there is no reflection on the glass surface, GSDNet [3] will under-detect the glass surface at the right side of the scene, and even humans is hard to distinguish whether there is glass at the rightmost glass-like region. However, while a flash is applied in the same scene, the appearance of a reflection prompts our method to identify the glass surface, which highlights the importance of applying a flash. Additionally, as shown in the 3rd scene, after applying the flash, the original obvious reflection on the glass surface disappears, while the non-glass homogeneous region in the left side of the image does not exhibit such an obvious difference.

In this paper, we propose a No-flash and Flash Glass Surface Detection Network (NFGlassNet), which contains two novel modules: Reflection Contrast Mining Module (RCMM) for accurately extracting reflections from non-flash and flash image pairs, and Reflection Guided Attention Module (RGAM) for identifying glass surface guided by the extracted reflection cues. In addition, for learning our NFGlassNet, we construct a large scale No-flash and Flash Glass Surface Dataset (NFGD) based on the reflection dynamics (appearance and disappearance) in flash/no-flash imagery, which consists of approximately 3.3k no-flash and flash image pairs captured with a Canon EOS 80D equipped with a flash. Unlike existing no-flash and flash datasets [15]-[17] proposed for low-level

tasks (e.g., reflection removal [16], [17], [55], denoising [15]), our NFGD contains a large number of glass surface instances across diverse scenes. Notably, for deploying our method, a program can be customed to control the target camera (e.g., phone) to capture no-flash and flash image pairs in sequence (no-flash shot followed by a flash shot).

In general, the main contributions of our work can be summarized as follows:

- We propose a novel network, called *NFGlassNet*, which leverages the reflection dynamics present in flash/no-flash imagery for glass surface detection.
- We propose a Reflection Contrast Mining Module (RCMM) for extracting reflection from non-flash and flash image pairs, and a Reflection Guided Attention Module (RGAM) for accurately detecting glass surfaces guided by the reflection cues.
- We construct a new glass surface detection dataset, named NFGD, consisting of 3312 no-flash and flash image pairs along with corresponding annotations.
- Extensive experiments conducted on various real-world scenes demonstrate the superior performance of our method compared with the state-of-the-art methods.

II. RELATED WORK

A. Glass Surface Detection

Mei et al. [1] first proposed the glass surface detection problem and explored contextual glass features from a large receptive field. He et al. [4] focused on glass boundary information and proposed a point-based graph convolution module to accurately distinguish between glass and non-glass regions. Yu et al. [5] leveraged a mutual guidance approach between high-level and low-level features to obtain more accurate glass features for refining the glass mask. Lin et al. [3] considered the intrinsic properties of glass and first utilized reflection cues for glass surface detection. Furthermore, Yan et al. [7] proposed to leverage ghosting effect appeared on glass surfaces to accurately detect glass surfaces. Qi et al. [6] noted that Gaussian blurriness is a unique property of glass surfaces and utilized average pooling to simulate this property for glass surface detection. However, these previous methods based on single images may fail when these glass cues disappear (e.g., unclear glass boundaries, absence of reflections on the glass surface, image blur, etc.).

Recently, Lin et al. [54] proposed an RGB-D glass surface detection method based on the phenomenon of depth missing in glass regions. Mei et al. [10] proposed an RGB-P glass surface detection method based on the polarization cues of glass surfaces. Lin et al. [12] observed that glass surfaces are usually accompanied by walls or curtains, leading to a semantics-prior method (RGB-S) based on the contextual information around glass surfaces. Huo et al. [14] noted that the thermal conductivity of glass differs from that of other materials, thus utilizing an extra thermal sensor (RGB-T) to locate glass surface regions. Yan et al. [13] recognized that near-infrared can effectively suppress reflections on glass surfaces, and propose NRGlassNet, which takes as input RGB-NIR image pairs for glass detection. Although these multi-



Fig. 3. Comparison between GSD [3], GSGD [7] and our NFGD. Each no-flash and flash image pair from our NFGD exhibits the appearance and disappearance phenomenon of reflections on glass surfaces. Our NFGD encompasses a wide range of shots across various real-world scenes.

modal methods improve detection performance, additional sensors often incur high costs and require pixel alignment between the two modalities. Our method (RGB-Flash) can fully utilize reflection cues from no-flash and flash image pairs to detect glass surfaces without extra costs and preprocessing.

B. Transparent Object Detection

Xie et al. [2], [35] proposed a convolution-based network named TransLab [2] and a convolution union transformerbased network named Trans2Seg [35] for transparent object detection. They also constructed a large-scale dataset, Trans10K-V2 [35], which includes two categories of transparent objects, stuff and things. Zhang et al. [37] developed a dual prediction head utilizing a shared transformer-based encoder and non-shared decoders for deploying transparent object detection on mobile devices. Zhu et al. [38] and Liang et al. [39] aimed to reconstruct the depth missing regions caused by transparent objects in depth maps. They proposed a boundary-aware method and a line segment-prior method, respectively, to detect transparent objects before depth reconstruction. Moreover, there are also methods that explore boundary cues to improve detection from polarization [40] and light field [41] images. All these methods achieve good performance in transparent object detection, as transparent objects typically possess easily observable geometric boundaries. However, glass surfaces usually do not have this property, thus require prior effective cues to guide the detection of glass surfaces.

C. Mirror Detection

Mei et al. [42] first provided a large benchmark for mirror detection by utilizing the discontinuity of textures between mirror and non-mirror regions for mirror detection. Lin et al. [21] noted the strict symmetry of objects inside and outside the mirror, detecting the mirror by exploring the similarity between adjacent feature cells in the feature space. Huang et al. [43] further observed the loose symmetry of mirrors due to specific perspectives, and they explored this loose symmetry by using the image and its mirrored version as inputs to enhance mirror detection. Guan et al. [44] noted that mirrors often appear alongside sinks or dressers, proposing semantics as a prior for mirror detection. Tan et al. [45] leveraged the intrinsic visual properties of mirrors to facilitate mirror detection. Zha et al. [57] argued that the frequencies inside and outside the mirror are distinctive, and

exploited low-frequency features to locate the mirror region and high-frequency features to refine detection results. Xie *et al.* [22] further adopted the Discrete Cosine Transform (DCT) from a frequency perspective to extract mirror features across different frequency domains, improving the accuracy of mirror detection. However, unlike mirrors, glass surfaces do not have clear boundaries, and the reflection layer always mixed with corresponding transmission layer, causing mirror detection methods being less effective in serving glass detection.

D. Flash and No-flash Image Pairs for Computer Vision Tasks

Petschnigg et al. [70] proposed a variety of methods that analyze and combine the strengths of such flash/no-flash image pairs for image restoration and enhancement, such as Flash-to-ambient detail transfer and continuous flash intensity adjustment. Flash and No-flash image pairs have been also leveraged in saliency detection [67], reflection removal [72], and denoising image captured from low-light conditions [68], [69]. Moreover, Cao et al. [71] proposed a method for recovering shape and albedo of Lambertian surfaces from a stereo flash/no-flash pair. Notably, Maralan et al. [73] proposed a physically motivated intrinsic formulation for flash photograph formation, and developed flash decomposition and generation methods for flash and no-flash photographs, respectively. However, this method exhibits limited generalization ability and struggles to effectively process flash and no-flash photographs in the presence of glass surfaces.

III. NO-FLASH AND FLASH GLASS DATASET (NFGD)

Lin et al. [3] and Yan et al. [7] have proposed the GSD [3] and GSGD [7] for glass surface detection, images from which always contains prominent reflections on the glass surface. However, not every image in GSD exhibits reflections on glass surfaces. Moreover, close-up shots capture double-layer reflections (ghosting effects) in GSGD. For learning our network, we propose NFGD, which consists of ~3.3k no-flash and flash image pairs along with corresponding annotations. Our NFGD complements the scenes with a lack of reflections on glass surfaces in GSD, and offers a more varied range of shots (close-up, medium, and long shots) compared to GSGD. Several examples from each dataset exhibited in Fig. 3 demonstrate the superiority of our NFGD.

A. Dataset Construction

No-flash and flash image pairs from our NFGD are captured with a Canon 80D DSLR camera from various semantic scenes, including bathrooms, lounges, laboratories, hospitals, libraries, shopping malls, and schools. We also design a camera script to capture a pair of no-flash and flash images within a very short time, ensuring no pixel offset between the image pairs. To achieve greater variability in the illumination of images with flash, we captured images with different illuminations to enhance the robustness of our dataset. Specifically, we adjusted image brightness using varying flash intensities, aperture sizes, exposure times, and ISO settings. We also utilized an additional external hot-shoe flash (maximum brightness: 60 GN at ISO 100) to apply flash, using powers of $\times 1/2$, $\times 1/4$, and $\times 1/8$ to obtain different flash intensities. Our dataset encompasses scenes acquired under diverse ambient light conditions, including midday sunshine and overcast dusk. We prioritize adjusting the aperture size and exposure time to ensure the captured images accurately represent real-world observed brightness. This methodology enriches the dataset's scene diversity while preserving image fidelity.

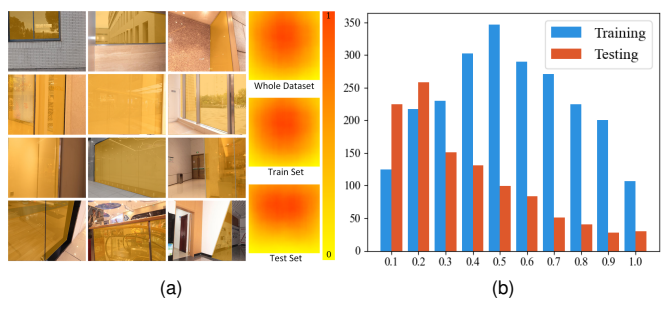


Fig. 4. Statistics of our NFGD. Fig. 4a Glass surface location distribution. Fig. 4b Ratio of glass area against image area.

B. Dataset Analysis

- Glass Location. The glass location distribution is the average of all glass surface regions in the dataset. We adopt the same method as [5], [10] to evaluate our NFGD. As shown in Fig. 4a, glass surfaces in our dataset primarily concentrate at the middle and top regions, which is consistent in training and testing sets. Moreover, we employed shots from different distances and at various tilt angles to diversify the locations and shapes of glass instances, which could avoid the "center bias" problem due to natural observation tendencies.
- Area Ratio. As mentioned in [3], this metric is defined as the ratio of the glass region size to the total image size, reflecting the additional context provided by the surrounding environment. In other words, a smaller glass region allows more room for the environment to offer supplementary hints. As shown in Fig. 4b, the majority of our training and testing sets are distributed within the 0 to 0.5 range, indicating that our dataset consists of relatively small glass regions, which is beneficial for the glass surface detection task.

IV. METHODOLOGY

In this section, we introduce our *NFGlassNet* for glass surface detection with the aid of cues from the appearance and disappearance phenomenon of reflections caused by a flash. In the first subsection, we present the overall pipeline of the network. In the second and third subsections, we elaborates on our Reflection Contrast Mining Module (RCMM) and Reflection Guided Attention Module (RGAM), respectively.

A. Overall Pipeline

For multimodal glass surface detection [9], [10], [13], [14], [54], mirror detection [9], [23] and salient object detection [58]–[64], images from auxiliary sensors often show significant semantic and textural differences compared to RGB counterparts. In each flash/no-flash image pair, semantic and texture information remains largely consistent, with the exception of reflection regions. Therefore, we do not need a complex encoder architecture like the multimodal mirror detection method [23] to fuse two modalities with significant differences in the encoder stage.

As illustrated in the Fig. 5, our network takes a pair of no-flash and flash images as input. It employs a pipeline consisting of encoder, extraction and fusion, and then decoder. Due to the diverse shapes and varying sizes of different glass surfaces, a large-field contextual exploration is essentially needed to acquire a more precise and robust detection of glass surfaces. Consequently, we utilize Swin-Transformer V2 [25] rather than ResNeXt [26] as the backbone network, as the former is better at modeling long-range dependencies.

Given the input no-flash and flash image pair $\mathbf{I}_{\text{no-flash}} \in \mathbb{R}^{H \times W \times 3}$ and $\mathbf{I}_{\text{flash}} \in \mathbb{R}^{H \times W \times 3}$, we extract feature sets $\mathbf{F}_{\text{no-flash}}$ and $\mathbf{F}_{\text{flash}}$ from them using two identical Swin-Transformer V2 [25] backbones without sharing weights. Specifically, the definitions of $\mathbf{F}_{\text{no-flash}} = \{\mathbf{F}_{\text{no-flash}}^i \in \mathbb{R}^{\frac{H}{2^{i-1}} \times \frac{W}{2^{i-1}} \times (C \times 2^{i-1})} \mid i \in \{1,2,3,4\}\}$ and $\mathbf{F}_{\text{flash}}$ are similar.

The features $\mathbf{F}_{\text{no-flash}}$ and $\mathbf{F}_{\text{flash}}$ are then fed into the RCMM group and RGAM group to extract and fuse features. Each group contains four layers of corresponding modules with different scales, where the input feature size of each layer adapts to the multi-scale features extracted from the encoder. In the RCMM group, $\mathbf{F}_{\text{no-flash}}$ and $\mathbf{F}_{\text{flash}}$ pass through the RCMM and yield the prediction of the reflection images $\mathbf{R}_{\text{no-flash}}$, $\mathbf{R}_{\text{flash}}$, and the reflection features $\mathbf{F}_{\text{refle}}$. These reflection features, along with $\mathbf{F}_{\text{no-flash}}$ and $\mathbf{F}_{\text{flash}}$, are then sent into RGAM group, where each RGAM adopts an optimized attention map to fuse reflection and glass features to obtain features more relevant to glass surfaces, denoted as \mathbf{F}_{RGAM} . Finally, a straightforward cascaded decoder is used to predict the final glass surface mask for the input image pair.

B. Reflection Contrast Mining Module (RCMM)

Fig. 1 shows that the distinct difference between the no-flash and flash images in the same scene lies in the appearance and disappearance of reflections. Therefore, we propose RCMM to extract reflection from the input non-flash and flash image pair, as shown in Fig. 6. First, a contrast branch in the middle

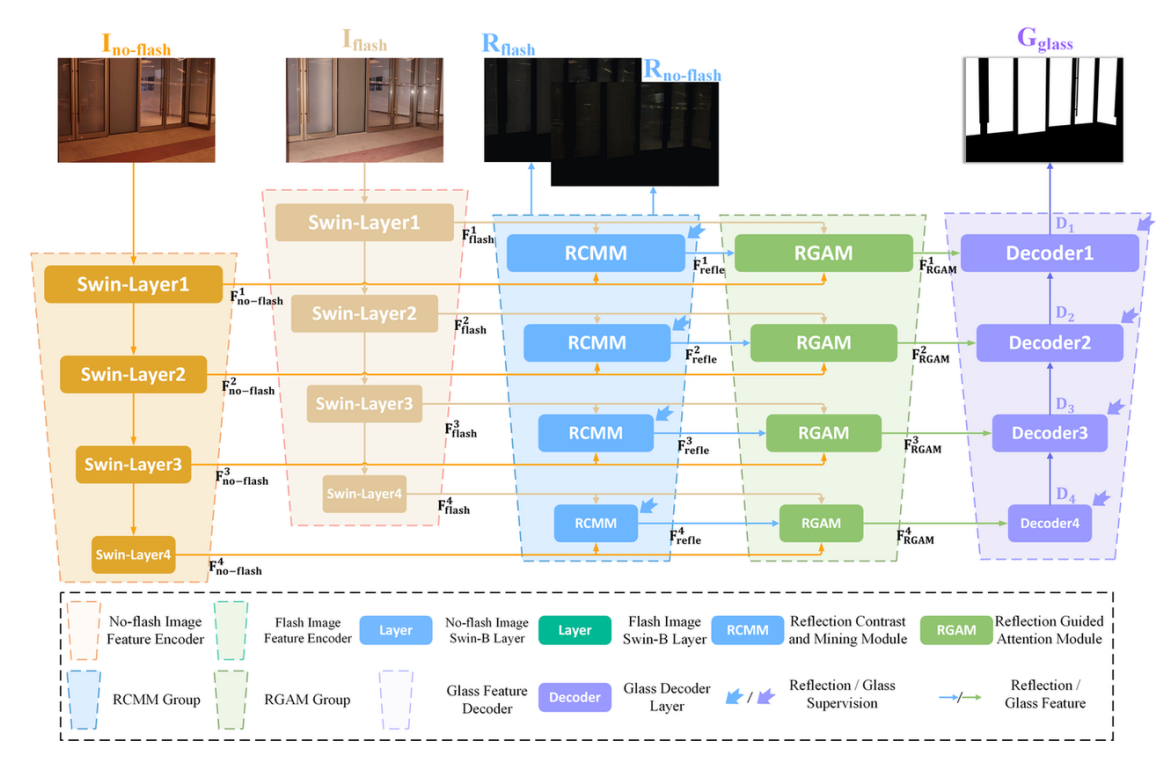


Fig. 5. The architecture of our proposed No-flash and Flash Glass Surface Detection Network (NFGlassNet).

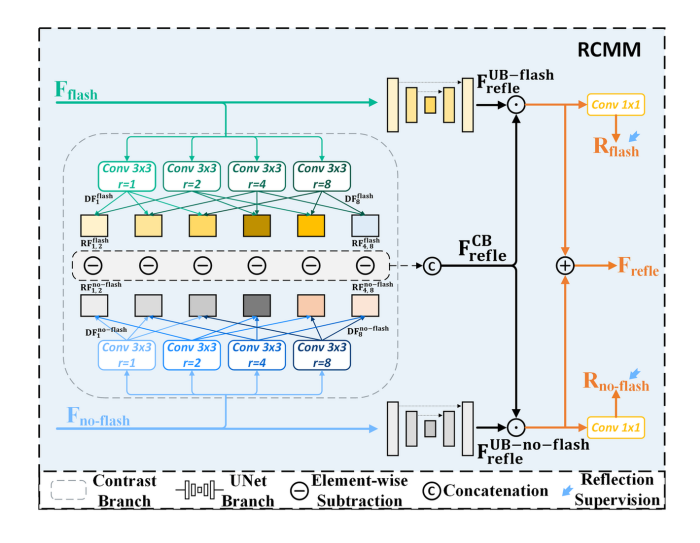


Fig. 6. The architecture of the Reflection Contrast Mining Module (RCMM).

of RCMM is used to captures the contrast difference (i.e., the reflections) between the no-flash image and the flash image by subtracting their feature maps. Second, two UNet branches are employed to extract reflections from each individual input image to complement the reflection features extracted by the contrast branch.

Reflections on glass surfaces don't have a fixed shape and exhibit a huge variation in scale. They can appear anywhere on the glass surface and blend with the transmission layer. Therefore, it is necessary to capture potential reflection using multiple receptive fields with different sizes. In our RCMM, $\mathbf{F}_{\text{no-flash}}$ and $\mathbf{F}_{\text{flash}}$ are fed to an array of dilated convolutions (denoted as $\mathrm{DConv}_{r_i}^{\mathrm{flash/no-flash}}(\cdot)$) with different dilation rates $\mathbf{r_i} \in \{1,2,4,8\}$ to capture features. The extracted features $\mathbf{DF}_{r_i}^{\mathrm{flash}}$ and $\mathbf{DF}_{r_i}^{\mathrm{no-flash}}$ can be expressed as:

$$\mathbf{DF}_{r_i}^{\text{flash}} = \mathrm{DConv}_{r_i}^{\text{flash}}(\mathbf{F}_{\text{flash}}),\tag{1}$$

$$\mathbf{DF}_{r_i}^{\text{flash}} = \mathrm{DConv}_{r_i}^{\text{flash}}(\mathbf{F}_{\text{flash}}), \tag{1}$$

$$\mathbf{DF}_{r_i}^{\text{no-flash}} = \mathrm{DConv}_{r_i}^{\text{no-flash}}(\mathbf{F}_{\text{no-flash}}). \tag{2}$$

These features are then fused pairwise according to their permutations as shown in Fig. 6 to obtain richer features from different receptive field size. The pairwise fused features from $\mathbf{F}_{\text{flash}}$ and $\mathbf{F}_{\text{no-flash}}$ are denoted as $\mathbf{RF}_{r_i,r_j}^{\text{flash}}$ and $\mathbf{RF}_{r_i,r_j}^{\text{no-flash}}$, respectively, and $\mathbf{RF}_{r_i,r_j}^{\text{flash}}$ can be defined as:

$$\mathbf{RF}^{\mathrm{flash}}_{r_i,r_j} = \mathbf{DF}^{\mathrm{flash}}_{r_i} + \mathbf{DF}^{\mathrm{flash}}_{r_j}, (r_i,r_j) \in \binom{\{1,2,4,8\}}{2}. \quad (3)$$

The definition for $\mathbf{RF}^{\text{no-flash}}_{r_i,r_j}$ is similar.

Subsequently, we subtract the features $\mathbf{RF}_{r_i,r_j}^{\mathrm{flash}}$ $\mathbf{RF}_{r_i,r_j}^{\text{no-flash}}$, which have the same dilation rate combination, in order to obtain differences. All differences from the corresponding dilation rate combination are then concatenated to produce the reflection features of the contrast branch $\mathbf{F}_{\text{refle}}^{\text{CB}}$. This process can be written as:

$$\mathbf{F}_{\text{refle}}^{\text{CB}} = \text{Concat}\left(\left\{\mathbf{R}\mathbf{F}_{r_i,r_j}^{\text{flash}} - \mathbf{R}\mathbf{F}_{r_i,r_j}^{\text{no-flash}}\right\}\right).$$
 (4)

On the other hand, we also directly extract reflections from $\mathbf{F}_{\text{no-flash}}$ and $\mathbf{F}_{\text{flash}}$ through the top and bottom branches of RCMM. Specifically, inspired by [27], we employ a simple UNet [53] (denoted as $\mathcal{U}^{\text{flash/no-flash}}(\cdot)$) to extract features of reflection from $\mathbf{F}_{\text{flash}}$ and $\mathbf{F}_{\text{no-flash}}$ as follows:

$$\mathbf{F}_{refle}^{UB\text{-flash}} = \mathcal{U}^{flash}(\mathbf{F}_{flash}), \tag{5}$$

and $\mathbf{F}_{refle}^{UB\text{-no-flash}}$ follows the same process.

In the final stage, these two types of reflection features are fused to produce the output reflection feature as follows:

$$\begin{split} \mathbf{F}_{\text{refle}} &= \mathbf{F}_{\text{refle}}^{\text{no-flash}} + \mathbf{F}_{\text{refle}}^{\text{flash}} \\ &= (\mathbf{F}_{\text{refle}}^{\text{CB}} \odot \mathbf{F}_{\text{refle}}^{\text{UB-flash}}) + (\mathbf{F}_{\text{refle}}^{\text{CB}} \odot \mathbf{F}_{\text{refle}}^{\text{UB-no-flash}}). \end{split} \tag{6}$$

Concurrently, we employ two 1x1 convolutional layers to extract corresponding reflection images \mathbf{R}_{flash} and $\mathbf{R}_{no\text{-}flash}$ from the features $\mathbf{F}_{\text{refle}}$ and $\mathbf{F}_{\text{no-refle}}$ respectively.

Pseudo Ground Truth for Reflection: To effectively supervise $\mathbf{F}_{\text{refle}}$, we generate the pseudo ground truth, $\hat{\mathbf{R}}_{\text{flash}}$ and $\hat{\mathbf{R}}_{\text{no-flash}}$ for the $\mathbf{R}_{\text{flash}}$ and $\mathbf{R}_{\text{no-flash}},$ respectively. The process diagram can be found in our supplemental. Existing SOTA reflection detection methods (e.g., LANet [19]) always assume that glass surfaces (or reflections) cover the entire image, while our method only cares about reflections on glass surfaces, which locate in local regions of the input image. Thus, existing reflection detection methods cannot be directly used to supervise the reflection cue extraction of our method, as shown in Fig. 7. Specifically, we first apply the ground-truth glass mask to cover the input image pair, and then adopt LANet [19] to obtain the pseudo ground-truth reflections $(\hat{R}_{no-flash}, \hat{R}_{flash})$ from the masked no-flash and flash images.

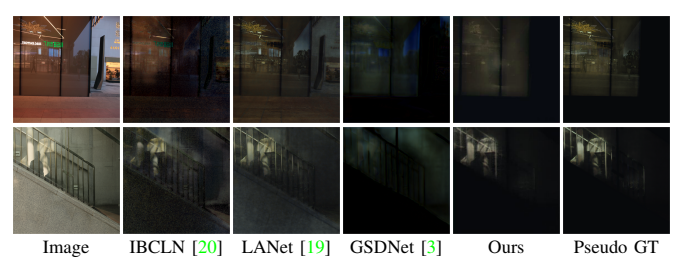


Fig. 7. Reflection extractions from two SOTA methods (IBCLN [20] and LANet [19]) in SIRR, and GSDNet [3] in glass surface detection. Note that all three methods mis-detect non-glass regions as glass reflections, and reflections of GSDNet [3] are too weak in real scenes. Our method is able to correctly detect reflections in these challenging scenes.

C. Reflection Guided Attention Module (RGAM)

As shown in Fig. 8, our RGAM aims to fuse the extracted reflection features and features extracted from no-flash and flash images. Thus, to fully explore the two kinds of features, we adopt dual cross-attention branches to independently search for reflection features (\mathbf{F}_{refle}) from the concatenated feature (\mathbf{F}_{glass}) of $\mathbf{F}_{no\text{-flash}}$ and \mathbf{F}_{flash} , and the concatenated features (\mathbf{F}_{glass}) from the reflection features (\mathbf{F}_{refle}) . In this way, two attention maps named M_{refle} and M_{glass} can be obtained.

Reflections can appear on various smooth surfaces, and some glass-like regions have smooth surfaces and frames that resemble the borders of glass surfaces are easily mistaken for glass surface. Therefore, we multiply the two attention maps $\mathbf{M}_{\text{refle}}$ and $\mathbf{M}_{\text{class}}$ obtained from the top and bottom branches (cross-attentions) to obtain the enhanced (shared) attention map M_{shared} . This enhanced attention map is then multiplied back to each branches to obtain the refined features. Finally, the features from the two branches are added to produce the final fused feature \mathbf{F}_{RGAM} .

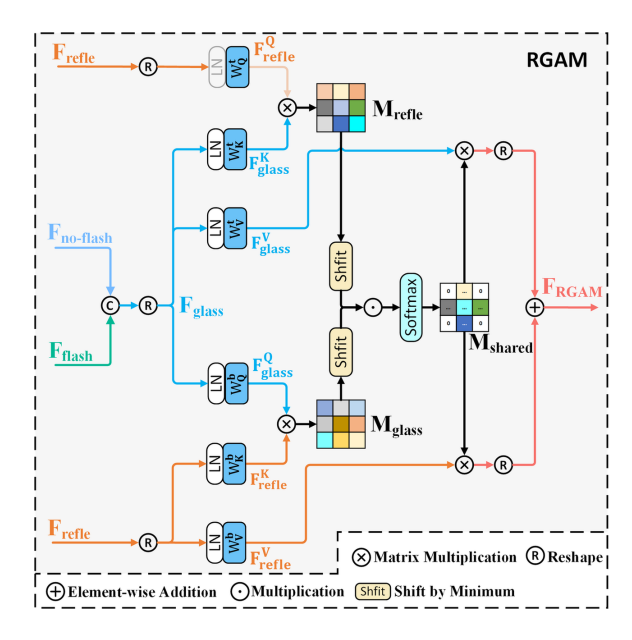


Fig. 8. The architecture of our Reflection Guided Attention Module (RGAM).

Specifically, we employ two cross-attention in parallel, which allows the two features to serve as the query (\mathbf{Q}) in turn to ensure that the two query features (i.e., $\mathbf{F}_{\text{refle}}$ and \mathbf{F}_{glass}) are fully and equally explored. Unlike the serial singlebranch structure used by [28] for feature fusion, our parallel dual cross-attention branches avoid insufficient exploration of features due to the order of the two queries.

 \mathbf{F}_{glass} is the concatenation of \mathbf{F}_{flash} and $\mathbf{F}_{no-flash}$, defined as:

$$\mathbf{F}_{\text{glass}} = \text{Conv}_{1 \times 1}(\text{Concat}(\mathbf{F}_{\text{no-flash}} + \mathbf{F}_{\text{flash}})),$$
 (7)

where $Conv_{1\times 1}$ denotes the 1×1 point-wise convolution to adjust channel numbers.

Then, we reshape $\mathbf{F}_{\text{glass}}$ and $\mathbf{F}_{\text{refle}} \in \mathbb{R}^{\hat{H} \times \hat{W} \times \hat{C}}$ to $\mathbb{R}^{\hat{H}\hat{W}\times N\times \frac{C}{N}}$, where N is the number of heads in the multihead attention. After they pass through Layer Normalization $(LN(\cdot))$, two sets of learnable matrices with the same structure but non-shared weights $(W_Q^{\prime\prime b},\,W_K^{\prime\prime b},\,$ and $W_V^{\prime\prime b})$ are applied to generate their respective tokens. \mathbf{F}_{refle} and \mathbf{F}_{glass} take turns as the query (\mathbf{Q}). When \mathbf{F}_{refle} serves as the query (\mathbf{Q}), and $\mathbf{F}_{\text{glass}}$ serves as the key (**K**) and value (**V**), this process can be described as:

$$\mathbf{F}_{refle}^{Q} = W_{O}^{t}(LN(reshape(\mathbf{F}_{refle}))),$$
 (8)

$$\mathbf{F}_{\text{glass}}^{K} = W_{K}^{t}(\text{LN}(\text{reshape}(\mathbf{F}_{\text{glass}}))),$$
 (9)

$$\mathbf{F}_{glass}^{V} = \mathbf{W}_{V}^{t}(\mathrm{LN}(\mathrm{reshape}(\mathbf{F}_{glass}))).$$
 (10)

While \mathbf{F}_{glass} acts as the *query*, the process of obtaining \mathbf{F}_{glass}^Q , $\mathbf{F}_{\text{refle}}^{K}$ and $\mathbf{F}_{\text{refle}}^{V}$ through the bottom cross-attention follows the similar way.

Next, we can obtain attention maps $\mathbf{M}_{refle}, \mathbf{M}_{glass}$ \in $\mathbb{R}^{N imes \hat{H}\hat{W} imes \hat{H}\hat{W}}$ for $\mathbf{F}_{\text{refle}}$ and $\mathbf{F}_{\text{glass}}$, respectively, which can be

$$\mathbf{M}_{\text{refle}} = \mathbf{F}_{\text{refle}}^{Q} \otimes (\mathbf{F}_{\text{glass}}^{K})^{\text{T}}, \tag{11}$$

$$\mathbf{M}_{\text{glass}} = \mathbf{F}_{\text{glass}}^{Q} \otimes (\mathbf{F}_{\text{refle}}^{K})^{\text{T}}. \tag{12}$$

$$\mathbf{M}_{\text{glass}} = \mathbf{F}_{\text{glass}}^{\mathbf{Q}} \otimes (\mathbf{F}_{\text{refle}}^{\mathbf{K}})^{\mathbf{T}}.$$
 (12)

Subsequently, a shift operation is applied to \mathbf{M}_{refle} and \mathbf{M}_{glass} , respectively, where the minimum value is subtracted from all elements in the matrix in order to shift values to the positive range starting from 0. After this, the two shifted attention maps are multiplied element-wise and then normalized through the softmax function, which yields the final shared (enhanced) attention map (\mathbf{M}_{shared}). This process can be expressed as:

$$\begin{aligned} \mathbf{M}_{shared} &= \operatorname{softmax}((\mathbf{M}_{refle} - \operatorname{Min}(\mathbf{M}_{refle})) \\ & \odot (\mathbf{M}_{glass} - \operatorname{Min}(\mathbf{M}_{glass}))), \end{aligned} \tag{13}$$

where $\operatorname{Min}(\cdot)$ denotes the minimum value of the matrix. After the shift operation, the feature cells corresponding to regions that are similar to \mathbf{Q} have values close to 1, while those dissimilar to \mathbf{Q} have values close to 0. Since the elementwise multiplication of two feature cells with values close to 1 results in a value still near 1, while the multiplication of cells close to 0 results in values even closer to 0, regions exhibiting both reflection and glass frame features will have their feature cell values enhanced, while regions lacking both features will be suppressed. As a result, our shared attention map is better at enhancing features and suppressing noise than the two respective attention map.

Finally, we multiply $\mathbf{M}_{\text{shared}}$ back to $\mathbf{F}_{\text{glass}}^{\text{V}}$ and $\mathbf{F}_{\text{refle}}^{\text{V}}$, and reshape the results into $\mathbb{R}^{\hat{H} \times \hat{W} \times \hat{C}}$. Then, element-wise addition is performed to obtain the more refined glass feature \mathbf{F}_{RGAM} as follows:

$$\mathbf{F}_{\text{RGAM}} = \text{reshape}(\mathbf{M}_{\text{shared}} \otimes \mathbf{F}_{\text{glass}}^{\text{V}}) + \text{reshape}(\mathbf{M}_{\text{shared}} \otimes \mathbf{F}_{\text{refle}}^{\text{V}}).$$
(14)

D. Decoder

In order to accurately decode features (\mathbf{F}_{RGAM}) output by RGAMs to obtain the final refined glass mask, we propose a progressive decoder. Since the glass features have been sufficiently explored and fused in RCMM and RGAM, the decoder should be as simple as possible. Similar to GSD-Net [3] and PGSNet [5], we upsample ($\mathrm{Up}(\cdot)$) deep features and concatenate them with shallow features along the channel dimension to decode each layer's features, then pass the decoded features to even shallower layers. The process at each decoder layer (\mathbf{D}_i) can be represented as:

$$\mathbf{D}_{i} = \begin{cases} \operatorname{Conv}(\operatorname{Concat}(\operatorname{Up}(\mathbf{D}_{i+1}), \mathbf{F}_{\mathbf{RGAM}}^{i})) & i = 1, 2, 3 \\ \operatorname{Up}(\mathbf{F}_{\mathbf{RGAM}}^{4}) & i = 4, \end{cases}$$
(15)

where $\operatorname{Conv}(\cdot)$ denotes a 3×3 convolution. Then, we obtain the glass mask $\mathbf{G}_i = \operatorname{Conv}_{1\times 1}(\mathbf{D}_i)$ for $i\in\{1,2,3,4\}$ layers of the Decoder. Finally, we upsample and adjust the channels of \mathbf{D}_1 to acquire the final glass mask (\mathbf{G}_{glass}) as follows:

$$\mathbf{G}_{\text{glass}} = \text{Conv}(\text{Up}(\mathbf{D}_1)). \tag{16}$$

E. Loss Functions

Our loss function consists of supervision for the glass and reflection. The total loss \mathcal{L} can be expressed as:

$$\mathcal{L} = \sum_{i=1}^{4} (\mathcal{L}_{glass}(\mathbf{G}_{i}, \hat{\mathbf{G}}_{i}) + \lambda \sum_{i \in S} \mathcal{L}_{refle}(\mathbf{R}_{i}^{j}, \hat{\mathbf{R}}_{i}^{j})), \quad (17)$$

where λ is a hyper-parameter, $S = \{flash, no-flash\}$, and \mathbf{R}_{i}^{j} represents the reflection prediction decoded from $\mathbf{F}_{refle}^{flash}$ or $\mathbf{F}_{refle}^{no-flash}$ at each layer like CeilNet [18]. To supervise the reflection result, we adopt the SSIM loss and L_{1} loss, as:

$$\mathcal{L}_{refle}(\mathbf{R}_{i}^{j}, \hat{\mathbf{R}}_{i}^{j}) = 1 - SSIM(\mathbf{R}_{i}^{j}, \hat{\mathbf{R}}_{i}^{j}) + \|\mathbf{R}_{i}^{j} - \hat{\mathbf{R}}_{i}^{j}\|_{1}. \quad (18)$$

In order to obtain accurate glass surface regions and boundaries, we utilize IoU loss [31] and BCE loss [30] for glass supervision, as:

$$\mathcal{L}_{glass}(\mathbf{G}_{i}, \hat{\mathbf{G}}_{i}) = 1 - \frac{\mathbf{G}_{i}\hat{\mathbf{G}}_{i}}{\mathbf{G}_{i} + \hat{\mathbf{G}}_{i} - \mathbf{G}_{i}\hat{\mathbf{G}}_{i}} - (\hat{\mathbf{G}}_{i}\log\mathbf{G}_{i} + (1 - \hat{\mathbf{G}}_{i})\log(1 - \mathbf{G}_{i})). (19)$$

V. EXPERIMENTS

A. Experimental Settings

- 1) Implementation Details: We train our model using Py-Torch on an NVIDIA RTX 4090 GPU (24GB). We resize the no-flash and flash images to 384×384 for input and use Swin Transformer V2 [25] pre-trained on ImageNet [52] as our backbone network. We use the AdamW [48] optimizer with an initial learning rate of 1e-5. The batch size is set to 2, and the hyper-parameter λ is set to 0.8. We train our network for 150 epochs, which takes approximately 25 hours. The inference time for each image pair is around 0.2 seconds. To avoid overfitting, we apply the same data augmentation methods (e.g., random cropping, horizontal flipping, rotation) as the previous work [3] during training. Notably, we do not use CRF [49] for post-processing of the inferred images, as our method focuses more on correctly identifying glass and non-glass regions.
- 2) Evaluation Metrics: For evaluating our network with other competing methods comprehensively, we adopt five widely used metrics to assess the glass detection performance, including intersection over union (IoU), F-measure (F_{β}), mean absolute error (MAE), balanced error rate (BER), and pixel accuracy (ACC). The detailed formulations of these metrics can be further found in the supplementary material.

B. Comparison with the State-of-the-art Methods

1) Quantitative Comparison: As shown in Tab. I, 15 Stateof-the-art (SOTA) methods are chosen from the past five years for comparing with our method, including single image-based glass surface detection (GSD) methods [1]-[4], [7], multimodal image-based GSD methods [9], [10], [12]-[14], Salient Object Detection (SOD) methods [33], [34], [38], [58], [60], and Mirror Detection (MD) methods [21], [22]. We retrained these methods on our dataset with their codes, models, and corresponding training strategies to ensure a fair comparison. For all multimodal methods listed in Tab. I, we use the no-flash image as the RGB input and the flash image as the image from another modality. For the other comparison methods, we only use the no-flash image as the input in the training and inference process. The quantitative comparison results demonstrate a significant improvement over the baseline methods in all five evaluation metrics. In particular, our method performs better than the second-best method RGB-T [14] by IoU: 2.24%,

TABLE I

QUANTITATIVE COMPARISON BETWEEN OUR METHOD AND 17 STATE-OF-THE-ART METHODS FOR GLASS SURFACE DETECTION, SALIENT OBJECT

DETECTION, AND MIRROR DETECTION. WE REPORT IOU, F_{β} , MAE, BER, AND ACC VALUES. BEST AND SECOND-BEST RESULTS ARE MARKED IN RED

AND CYAN, RESPECTIVELY.

Task	Method	Year	IoU ↑	$F_{\beta}\uparrow$	$MAE\downarrow$	BER ↓	ACC ↑	Params(M)	FLOPs(G)
	Translab [2]	ECCV' 20	77.14	0.869	0.101	0.121	0.873	42.19	49.26
	GDNet [1]	CVPR' 20	78.83	0.872	0.097	0.115	0.881	207.95	231.50
Glass Detection (RGB-Only)	GSDNet [3]	CVPR' 21	80.21	0.887	0.094	0.108	0.887	83.71	92.86
	EBLNet [4]	ICCV' 21	79.92	0.878	0.096	0.115	0.885	111.71	322.16
	GhostingNet [7]	TPAMI' 24	81.98	0.898	0.088	0.096	0.899	280.33	322.33
	DGSDNet (RGB-D) [54]	AAAI' 25	81.14	0.890	0.092	0.091	0.890	80.54	35.06
	GlassSemNet (RGB-S) [12]	NeurIPS' 22	81.37	0.894	0.091	0.098	0.892	361.33	1412.03
Glass Surface Detection (Multimodal)	PGSNet (RGB-P) [10]	CVPR' 22	80.09	0.881	0.094	0.112	0.886	302.84	291.42
	RGB-T [14]	TIP' 23	83.93	0.909	0.065	0.072	0.912	81.25	42.68
	NRGlassNet (RGB-NIR) [13]	KBS' 24	82.85	0.899	0.083	0.085	0.903	203.37	195.07
	SPNet (RGB-D) [32]	ICCV' 21	82.68	0.897	0.083	0.089	0.898	81.05	202.74
	CIRNet (RGB-D) [33]	TIP' 22	82.93	0.894	0.077	0.081	0.903	103.16	42.60
SOD (Multimodal)	WaveNet (RGB-T) [34]	TIP' 23	83.74	0.902	0.065	0.069	0.909	84.88	64.02
	HENet (RGB-D) [58]	TCSVT' 24	74.32	0.849	0.156	0.145	0.868	10.43	10.75
	LASNet (RGB-T) [60]	TCSVT' 23	77.46	0.875	0.114	0.118	0.879	93.57	111.69
Mirror Detection	PMDNet [21]	CVPR' 21	80.95	0.886	0.093	0.103	0.891	147.66	119.27
Willfor Detection	CSFwinformer [22]	TIP' 24	83.86	0.903	0.068	0.079	0.904	188.62	209.83
Glass Surface Detection	Ours (RGB-Flash)	-	86.17	0.922	0.052	0.053	0.934	208.43	140.20

 F_{β} : 1.3%, MAE: 1.4%, BER: 1.9%, and ACC: 2.2%. The qualitative results of our method and competing methods evaluated on two multimodal datasets: RGB-T [14] and RGB-NIR [13] are shown in our supplementary material.

To validate whether good illumination intensity can improve the detection performance of the competing methods, we select five methods that performs well across different tasks. As shown in Tab. II, for evaluating GSDNet [3], GhostingNet [7] and CSFwinformer [22], we conduct experiments using only the flash image as input. For RGB-T [14] and WaveNet [34], the input setting is reversed compared to that of Tab. I, where we use the flash image as the RGB input and the no-flash image as the image from another modality. For our NFGlassNet, we reverse the input setting similarly. The results demonstrate that most competing methods do not benefit from the extra illumination enhancement, which maybe due to their inability to handle the additional noise enhanced by the flash. Although the CSFwinformer [22] method benefits from the flash image, the improvement is limited, with IoU increasing by only 0.12%.

In addition, we evaluate our method on the single-image glass-surface detection benchmarks GDD and GSD, with the results summarized in Table III. For fairness, we retrained all the methods on our device using the same training parameters and we retain the dual-branch network structure, where both branches take the same RGB image as input. On GDD, our network slightly outperforms GhostingNet across all metrics, achieving improvements in IoU $(0.88\uparrow)$, F_{β} $(0.003\uparrow)$, MAE $(0.02\downarrow)$, BER $(0.36\downarrow)$, and ACC $(0.14\uparrow)$. On the GSD dataset, our method shows a more notable performance gain over GhostingNet, with increases in IoU $(2.39\uparrow)$ and F_{β} $(0.020\uparrow)$, decreases in MAE $(0.11\downarrow)$ and BER $(0.47\downarrow)$, and only a marginal drop of 0.001 in ACC. The results demonstrate that our model is capable of handling single image-based glass surface detection.

Moreover, we also evaluate the performance of our network

on other multimodal datasets. Specifically, Tab. IV shows the quantitat ive results of our method and competing methods evaluated on two multimodal datasets: RGB-T [14] and RGB-NIR [13]. It demonstrated that our *NFGlassNet* ranks secondbest in these two datasets. The performance of our network is only weaker than that of the network specifically designed for the particular dataset. We have only selected a few methods that perform well on our dataset (exhibited in Tab. I) as the competing methods in this study.

TABLE II

STUDY OF THE ILLUMINATION INTENSITY EFFECTS ON THE FOUR
METHODS THAT PERFORMED WELL IN TAB. I. WE REPLACED THE
ORIGINAL NO-FLASH IMAGE WITH THE FLASH IMAGE AS INPUT OF THE

COMPETING METHODS [3], [7], [22]. FOR OUR METHOD AND THE MULTIMODAL IMAGE-BASED METHODS [14], [34], WE EXCHANGE THE ROLES OF THE TWO IMAGES OF EACH INPUT NO-FLASH AND FLASH IMAGE PAIR. RESULTS THAT ARE BETTER THAN THE CORRESPONDING VALUES EXHIBITED IN TAB. I ARE MARKED IN CYAN.

Task	Method	IoU↑	$F_{\beta} \uparrow$	$MAE\!\!\downarrow$	$BER\!\!\downarrow$	$ACC\!\!\uparrow$
GSD	GSDNet [3] GhostingNet [7]	78.61 81.53	0.871 0.894	0.098 0.092	0.119 0.097	0.878 0.892
SOD	RGB-T [14] WaveNet [47]	83.41 83.26	0.901 0.901	0.069 0.070	0.076 0.075	0.908 0.905
MD	CSFWinformer [22]	83.98	0.912	0.067	0.070	0.906
GSD	Ours	86.14	0.923	0.054	0.058	0.934

2) Qualitative Comparison: As shown in Fig. 9, we compare our method with 7 SOTA methods [1], [3], [9], [12]–[14], [22]. The 1st scene shows that the bottom-left glass surface without a complete window frame in the no-flash image would be under-detected by GDNet [1], GSDNet [3] and RGB-D [9]. The 2nd, 3rd, 4th and 5th scenes show that most methods misdetect the rectangular frame (e.g., the rightmost open door shop in the 2nd scene, the bottom-right rectangular region in the 3rd scene, and the wall and floor near the glass frame in the 5th scene) as a glass region, as they have shapes similar to that of glass surfaces.

TABLE III

QUANTITATIVE COMPARISON BETWEEN OUR METHOD AND 7 STATE-OF-THE-ART METHODS ON THE SINGLE-IMAGE GLASS SURFACE DETECTION (GSD)

DATASETS, GDD AND GSD. TOD DENOTS TRANSPARENT OBJECT DETECTION. BEST DETECTION RESULTS ARE MARKED IN **bold**.

Task Method		Venue	GDD [1]				GSD [3]					
1ask Wieniou	venue	IoU↑	$F_{eta}{\uparrow}$	MAE↓	BER↓	ACC↑	IoU↑	$F_{eta} \uparrow$	MAE↓	BER↓	ACC↑	
GSD	GDNet [1]	CVPR'20	81.47	0.895	0.098	8.73	0.919	76.77	0.864	0.076	9.66	0.882
GSD	GSDNet [3]	CVPR'21	88.07	0.932	0.059	5.71	0.949	83.67	0.903	0.055	6.12	0.931
GSD	EBLNet [4]	ICCV'21	88.72	0.940	0.055	5.36	0.944	82.34	0.889	0.064	7.33	0.911
GSD	RFENet [74]	IJCAI'23	86.93	0.928	0.067	6.47	0.932	83.59	0.904	0.049	6.41	0.914
GSD	GhostingNet [7]	TPAMI'25	89.30	0.943	0.054	5.13	0.944	83.77	0.904	0.055	6.06	0.928
TOD	TransLab [2]	ECCV'20	81.97	0.899	0.095	8.98	0.920	74.23	0.837	0.089	10.40	0.886
TOD	Trans2Seg [35]	IJCAI'21	82.39	0.891	0.094	9.03	0.923	76.97	0.848	0.088	9.64	0.902
GSD	ours	-	90.18	0.946	0.052	4.77	0.958	86.16	0.924	0.044	5.59	0.927

The 6th and 7th scenes show challenging examples where glass surface frames are difficult to identify. GDNet [1], CSFWinformer [22], RGB-S [12], and RGB-D [9] underdetect glass surfaces, because the boundaries of the handrail and door are confusing and misleading. Since the boundary of the glass surface in the 8th scene is transparent, GDNet [1], RGB-S [12] and RGB-D [9] under-detect the glass surface in this scene.

In the 9th scene, the complex and unique appearance of the rightmost glass surface compared to other glass surfaces confuses GDNet [1], RGB-S [12] and RGB-D [9], which may be due to these methods cannot exploit reflection cues. The last scene shows a complex background behind the glass surfaces, with a billboard in front of the glass surface on the left side of the image. Moreover, the billboard with appearance similar to the background fools most competing methods.

These examples demonstrate that our method is able to accurately detect glass surfaces by exploiting the appearance and disappearance of reflections appeared on glass surfaces from the no-flash and flash image pairs. In contrast, competing methods always fail in these challenging scenes due to the lack of other obvious glass cues.

As shown in Fig. 11, we also visualize some intermediate results of our modules using heat maps. We can observe that the output features from the backbone $(F_{no-flash}^3)$ are rough and random. After passing through the RCMM, the output features (F_{refle}^3) are able to highlight the reflection regions. After passing through RGAM, the regions that contain

both reflections and glass frames are further highlighted in the output features (F_{RGAM}^3), which indicates the location of the glass surface. Finally, after passing through the decoder modules, the highlighted features in (D_3) are closer to the glass surfaces through the cascade feature decoding.

C. Ablation Studies

We conduct ablation studies on our proposed NFGlassNet to validate the effectiveness of the key modules, as shown in Tab. V. "Base" refers to the variant of our network after removing all the RCMMs and RGAMs. Then, we add either RCMM or RGAM to the "Base" model, which results in an improvement of IoU metric by 2.89% and 0.28%, respectively. The significant performance improvement brought by RCMM demonstrates the effectiveness of reflection cues in glass surface detection. Additionally, we replace RCMM with dual UNet, and RGAM with CBAM [51], respectively, in our model. Then, the IoU value drops by 1.90\% and 1.18%, respectively, compared to our complete model. This demonstrates the rationality and effectiveness of our network. Visual examples of incorporating the RCMM and RGAM are shown in Fig. 10. Further ablation study on the structure of RCMM and RGAM are reported in the rest of this subsection.

1) Effectiveness of the RCMM: As shown in Tab. VI, we conduct an ablation study on the structure of RCMM. B shows a larger drop in performance than A, which indicates that the contrast branch (Eq. 4) plays a more important role

TABLE IV

QUALITATIVE RESULTS OF OUR METHOD AND THE COMPETING METHODS EVALUATED ON THE RGB-T DATASET [14] AND THE RGB-NIR
DATASET [13]. THE BEST AND SECOND-BEST RESULTS ARE MARKED IN RED AND CYAN, RESPECTIVELY.

			RGB-T [14]				RGB-NIR [13]					
Modality Meth	Method	Task	IoU↑	$F_{\beta}\uparrow$	MAE↓	BER↓	ACC↑	IoU↑	$F_{\beta}\uparrow$	MAE↓	BER↓	ACC↑
RGB-T	RGB-T [14] WaveNet [47] SPNet [66]	GSD SOD SOD	87.13 84.84 79.52	0.911 0.902 0.882	0.026 0.046 0.093	0.037 0.046 0.064	0.895 0.880 0.844	85.36 86.48 83.23	0.922 0.927 0.908	0.056 0.052 0.065	0.057 0.052 0.062	0.952 0.960 0.942
RGB-D	PDNet [9] CIRNet [47]	MD SOD	81.12 83.26	0.883 0.901	0.076 0.070	0.063 0.075	0.881 0.905	84.62 83.07	0.921 0.913	0.058 0.098	0.058 0.066	0.947 0.931
RGB-NIR	NRGlassNet [13]	GSD	85.06	0.898	0.043	0.048	0.889	89.81	0.941	0.038	0.040	0.974
RGB-Flash	Ours	GSD	85.30	0.903	0.040	0.042	0.891	88.39	0.934	0.043	0.044	0.966

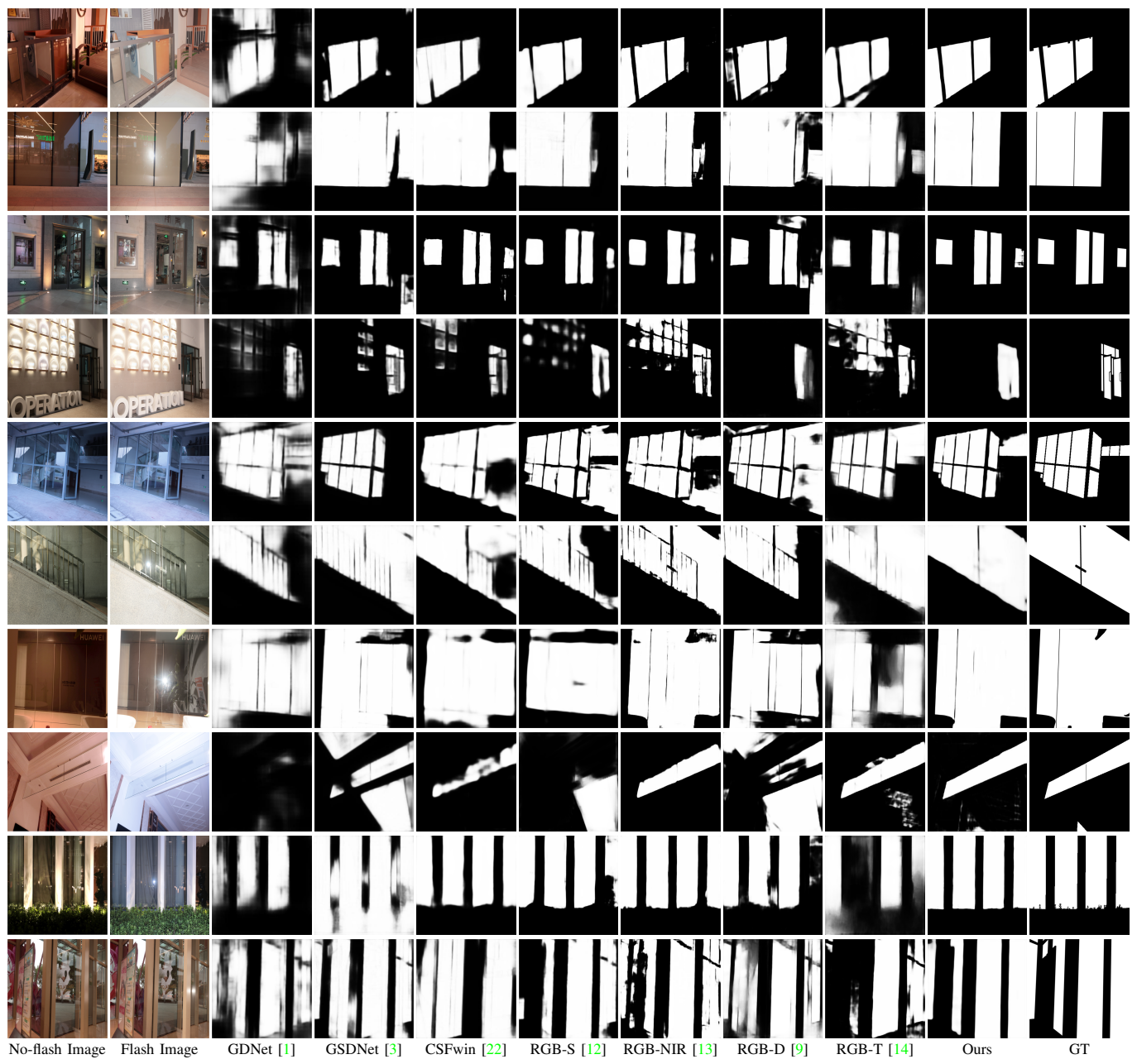


Fig. 9. Visual comparison of the glass surface detection results against state-of-the-art methods on our NFGD dataset. The first three methods based on single (i.e., no-flash) image detection, while the next four methods are multimodal detection methods (with the flash image as another modality input).

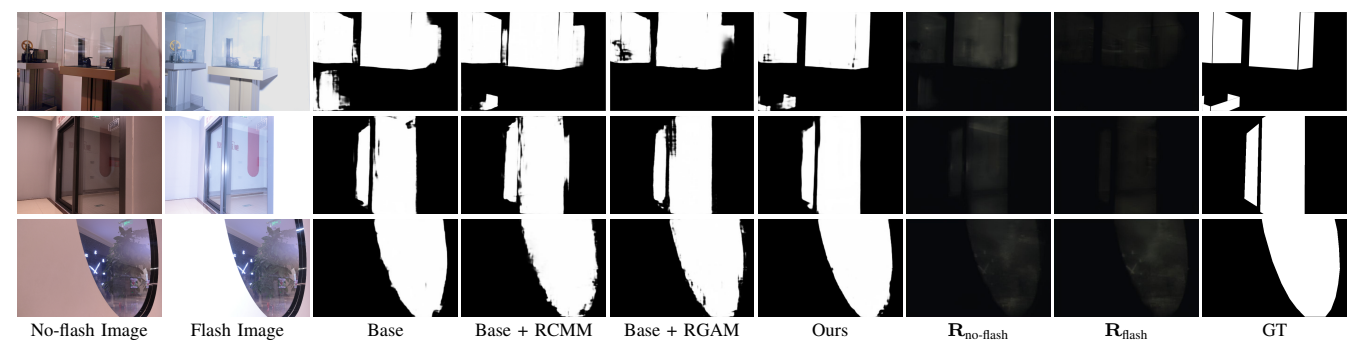


Fig. 10. Visual examples of the ablation study. The "Base" model means the variation of our *NFGlassNet* without RCMMs and RGAMs, which is prone to over-detection in most scenes. While incorporating RCMMs, the model can utilize reflection cues to locate glass regions, thereby reducing over-detection. The variation of our network ("Base + RGAM") can reduce mis-detecting glass-like rectangular areas glass surfaces. Our complete network (Base + RCMM + RGAM) performs best in all scenes.

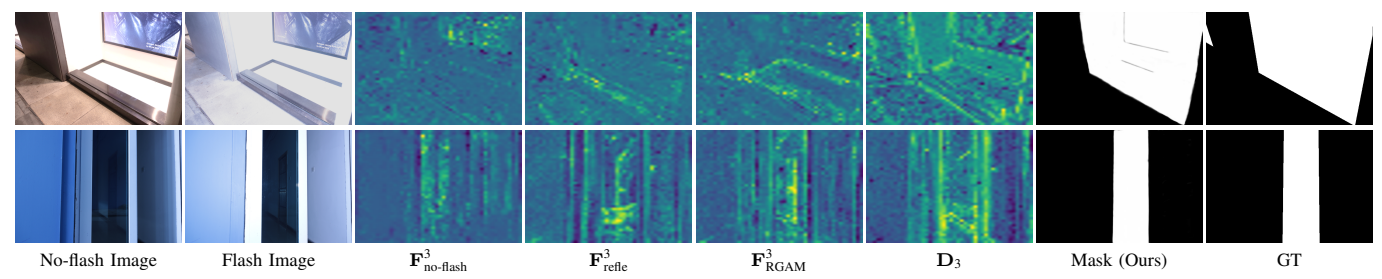


Fig. 11. Visual heat maps of the output features of key modules in our network.

TABLE V

ABLATION STUDY OF OUR METHOD (RCMM AND RGAM) ON OUR NFGD DATASET. "BASE" REFERS TO THE NO-FLASH AND FLASH BACKBONE NETWORKS WITH DECODERS, EXCLUDING RCMM AND RGAM. IN "BASE+RGAM," WE UTILIZED THE INFERRED REFLECTION RESULTS FROM LANET, THEN ENCODED THEM TO MATCH THE DIMENSIONS AND CHANNEL NUMBERS OF RCMM'S OUTPUT TO REPLACE RGAM'S ORIGINAL INPUT.

Method	IoU↑	$F_{\beta}\uparrow$	MAE↓	BER↓	ACC↑
Base	81.96	0.897	0.091	0.095	0.896
Base + RCMM	84.85	0.914	0.061	0.076	0.916
Base + RGAM	82.24	0.902	0.086	0.089	0.899
Base + dual UNet + RGAM	84.27	0.905	0.061	0.074	0.913
Base + RCMM + CBAM [51]	84.99	0.914	0.059	0.071	0.921
Base + RCMM + RGAM (Ours)	86.17	0.922	0.052	0.053	0.934

in reflection extraction than the UNet branch (Eq. 5). C demonstrates that RCMM without permutation addition (Eq. 3) results in a performance decrease, as more complementary information could interact during this step. D shows that replacing feature addition with feature subtraction significantly reduces the performance of RCMM, which proves the importance of difference extraction through feature subtraction (Eq. 4).

TABLE VI

ABLATION STUDY OF BLOCKS ON THE PROPOSED RCMM. "RCMM W/O UNET BRANCH" REFERS TO RCMM WITHOUT USING TWO UNET BRANCHES. "RCMM W/O CONTRAST BRANCH" DOES NOT USE CONTRAST BRANCH FOR DIFFERENCE EXTRACTION. "RCMM W/O PERMUTATION ADDITION" DOES NOT USE RICH DIFFERENCE FEATURES BUT INSTEAD USES SINGLE FEATURES FROM EACH CONVOLUTION DIRECTLY. "SUBTRACTION—ADDITION" REPLACES RICH DIFFERENCE FEATURE SUBTRACTION WITH FEATURE ADDITION.

Method	IoU↑	$F_{\beta} \uparrow$	MAE↓	BER↓	ACC↑
A w/o UNet branch B w/o contrast branch			0.053 0.061		
C w/o permutation addition D subtraction \rightarrow addition					
E Ours	86.17	0.922	0.052	0.053	0.934

2) Effectiveness of the RGAM: Similarly, we conduct ablation experiments on RGAM. As shown in Tab. VII, the comparison between A and G demonstrates that $\mathbf{M}_{\text{shared}}$ (Eq. 13) effectively fuses features between glass and reflection. B and G show that alternately using $\mathbf{F}_{\text{glass}}^{\mathbf{Q}}$ and $\mathbf{F}_{\text{refle}}^{\mathbf{Q}}$ (Eq. 8) as queries significantly improves detection performance, with glass features as the query bringing a greater benefit. D indicates that parallel branches, compared to serial branches, better facilitate feature fusion. The comparison between E and G demonstrates that shift operator (Eq. 13) improves the

detection performance, as it effectively enhances the glass surface features. F shows that the negative value features before shifting have a minor improvement on detection.

TABLE VII

Ablation study of blocks on the proposed RGAM. " $M_{SHARED} \rightarrow M_{RELFE}$, M_{GLASS} " refers to RGAM without using shared attention map but use dual cross attention with two attention maps respectively. "RGAM w/o alternate \mathbf{Q} ($\mathbf{F}_{GLASS}^{\mathbf{Q}}/\mathbf{F}_{REFLE}^{\mathbf{Q}}$ only)" does not let \mathbf{F}_{GLASS} and \mathbf{F}_{REFLE} " take turns as the \mathbf{Q} , and instead, $\mathbf{F}_{GLASS}/\mathbf{F}_{REFLE}$ serves as the \mathbf{Q} twice. "Parallel branch—series branch" replaces dual parallel cross attention branches with single series cross attention branch like [28] and $\mathbf{F}_{GLASS}^{\mathbf{Q}}$ is linked in series before $\mathbf{F}_{REFLE}^{\mathbf{Q}}$. "Shift—relu" replaces shift with relu function.

Method	IoU↑	$F_{\beta}\uparrow$	MAE↓	BER↓	ACC↑
$A \mathbf{M}_{\text{shared}} o \mathbf{M}_{\text{relfe}}, \mathbf{M}_{\text{glass}}$	85.48	0.916	0.059	0.062	0.927
B w/o alternate \mathbf{Q} ($\mathbf{F}_{\mathrm{glass}}^{\mathbf{Q}}$ only)	85.26	0.915	0.054	0.069	0.923
C w/o alternate \mathbf{Q} ($\mathbf{F}_{refle}^{\mathbf{Q}}$ only) D parallel branch \rightarrow series branch	84.89	0.910	0.063	0.076	0.917
D parallel branch→series branch	84.97	0.914	0.060	0.075	0.919
E w/o shift	85.35	0.916	0.056	0.060	0.921
F shift \rightarrow relu	85.93	0.919	0.058	0.059	0.929
G Ours	86.17	0.922	0.052	0.053	0.934

3) Effectiveness of the Loss Terms: As shown in Tab. VIII, we conduct an ablation study on the loss terms of our method. We observe that merely supervising the estimated reflections, but not supervising the predicted glass surface mask, significantly reduces the performance of our model. On the other hand, just going to supervise the predicted glass surface mask, but not supervising the estimated reflections, also weakens the performance of our method. which indirectly proves the importance of reflection cues for our method.

\mathcal{L}_{glass}	$\mathcal{L}_{refle}^{ ext{flash}}$	$\mathcal{L}_{refle}^{ ext{no-flash}}$	IoU↑	$F_{\beta} \uparrow$	MAE↓	BER↓	ACC↑
√			82.21	0.897	0.088	0.091	0.900
	\checkmark		73.47	0.849	0.088 0.109	0.148	0.825
		\checkmark	73.60	0.853	0.109	0.143	0.831
\checkmark	\checkmark		86.11	0.922	0.053 0.052	0.055	0.933
		✓	86.15	0.921	0.052	0.054	0.935
✓	✓	✓	86.17	0.922	0.052	0.053	0.934

D. Failure Cases

Our method does have limitations in some challenging scenes. As shown in the 1st scene of Fig. 12, our method over-detects the smooth floor tile as glass surface, as these glass-like floor tile share similar reflections and shapes as glass surfaces. Similarly, in the 2nd scene, the glass-like wall tiles

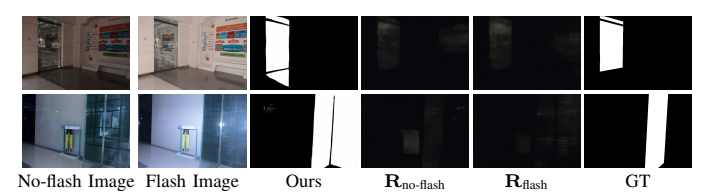


Fig. 12. Failure cases: our method may over-detect glass regions in some challenging scenes. In the two scenes above, our method mis-detected smooth tiles as glass surfaces, as the prominent reflections on their surfaces may confuse our method.

on the right side of the image having prominent reflection is mis-detected as glass surface by our method. Incorporating additional sensors may help solve such a problem.

VI. CONCLUSION

In this paper, we observed that in most real-world scenes, the illumination intensity in front of the glass surface differs from that behind it, which leads to variations in the reflections visible on the glass. Based on this phenomenon, we have proposed a novel method, *NFGlassNet*, for glass surface detection, which takes no-flash and flash image pairs as input. Specially, we proposed a Reflection Contrast Mining Module (RCMM) for extracting reflections, and a Reflection Guided Attention Module (RGAM) for fusing features from reflection and glass surface for accurate glass surface detection.

For learning our network, we have also proposed a noflash and flash image pair dataset (NFGD), which contains approximately 3312 image pairs along with the corresponding ground truth annotations. Extensive experiments demonstrate that our method effectively extracts and exploits reflection cues to identify glass surfaces and outperforms existing state-of-theart methods on our dataset.

In future work, we plan to leverage specialized sensors to improve our method, as our method may struggle with smooth non-glass surfaces that have prominent reflections. Moreover, we aim to extend our method to video-based glass surface detection, as motion cues from reflections in video could be further exploited to enhance detection performance.

REFERENCES

- [1] H. Mei, X. Yang, Y. Wang, Y. Liu, S. He, Q. Zhang, X. Wei, and R. W. Lau, "Don't hit me! glass detection in real-world scenes," in <u>CVPR</u>, 2020. 1, 2, 7, 8, 9, 10
- [2] E. Xie, W. Wang, W. Wang, M. Ding, C. Shen, and P. Luo, "Segmenting transparent objects in the wild," in ECCV, 2020. 3, 7, 8, 9
- [3] J. Lin, Z. He, and R. W. Lau, "Rich context aggregation with reflection prior for glass surface detection," in <u>CVPR</u>, 2021. 1, 2, 3, 4, 6, 7, 8, 9, 10
- [4] H. He, X. Li, G. Cheng, J. Shi, Y. Tong, G. Meng, V. Prinet, and L. Weng, "Enhanced boundary learning for glass-like object segmentation," in <u>CVPR</u>, 2021. 1, 2, 7, 8, 9
- [5] L. Yu, H. Mei, W. Dong, Z. Wei, L. Zhu, Y. Wang, and X. Yang, "Progressive glass segmentation," <u>IEEE Trans. on Image Processing</u>, vol. 31, 2022. 1, 2, 4, 7
- [6] F. Qi, X. Tan, Z. Zhang, M. Chen, Y. Xie, and L. Ma, "Glass makes blurs: Learning the visual blurriness for glass surface detection," <u>IEEE Trans. on Industrial Informatics</u>, vol. 20, no. 4, pp. 6631–6641, 2024.
- [7] T. Yan, J. Gao, K. Xu, X. Zhu, H. Huang, H. Li, B. Wah, and R. W. H. Lau, "Ghostingnet: A novel approach for glass surface detection with ghosting cues," <u>IEEE Trans. on Pattern Analysis and Machine Intelligence</u>, vol. 47, no. 1, pp. 323–337, 2025. 1, 2, 3, 7, 8, 9

- [8] J. Hao, M. Liu, J. Yang, and K. F. Hung, "Gem: Boost simple network for glass surface segmentation via vision foundation models," <u>IEEE</u> <u>Trans. on Multimedia</u>, pp. 1–13, 2025.
- [9] H. Mei, B. Dong, W. Dong, P. Peers, X. Yang, Q. Zhang, and X. Wei, "Depth-aware mirror segmentation," in CVPR, 2021. 4, 7, 8, 9, 10
- [10] H. Mei, B. Dong, W. Dong, J. Yang, S.-H. Baek, F. Heide, P. Peers, X. Wei, and X. Yang, "Glass segmentation using intensity and spectral polarization cues," in CVPR, 2022. 1, 2, 4, 7, 8
- [11] J. Lin, Y. H. Yeung, and R. W. Lau, "Depth-aware glass surface detection with cross-modal context mining," arXiv:2206.11250, 2022.
- [12] J. Lin, Y.-H. Yeung, and R. Lau, "Exploiting semantic relations for glass surface detection," in NeurIPS, 2022. 2, 7, 8, 9, 10
- [13] T. Yan, S. Xu, H. Huang, H. Li, L. Tan, X. Chang, and R. W. Lau, "Nrglassnet: Glass surface detection from visible and near-infrared image pairs," <u>Knowledge-Based Systems</u>, vol. 294, p. 111722, 2024. 1, 2, 4, 7, 8, 9, 10
- [14] D. Huo, J. Wang, Y. Qian, and Y.-H. Yang, "Glass segmentation with rgb-thermal image pairs," IEEE Trans. on Image Processing, vol. 32, pp. 1911–1926, 2023. 1, 2, 4, 7, 8, 9, 10
- [15] Y. Aksoy, C. Kim, P. Kellnhofer, S. Paris, M. Elgharib, M. Pollefeys, and W. Matusik, "A dataset of flash and ambient illumination pairs from the crowd," in ECCV, 2018.
- [16] C. Lei and Q. Chen, "Robust reflection removal with reflection-free flash-only cues," in CVPR, 2021. 2
- [17] Y. Hong, Y. Chang, J. Liang, L. Ma, T. Huang, and B. Shi, "Light flickering guided reflection removal," <u>International Journal of Computer Vision</u>, vol. 132, p. 3933–3953, 2024.
- [18] Q. Fan, J. Yang, G. Hua, B. Chen, and D. Wipf, "A generic deep architecture for single image reflection removal and image smoothing," in ICCV, 2017. 7
- [19] Z. Dong, K. Xu, Y. Yang, H. Bao, W. Xu, and R. W. Lau, "Location-aware single image reflection removal," in ICCV, 2021. 6
- [20] C. Li, Y. Yang, K. He, S. Lin, and J. E. Hopcroft, "Single image reflection removal through cascaded refinement," in CVPR, 2020. 6
- [21] J. Lin, G. Wang, and R. W. Lau, "Progressive mirror detection," in CVPR, 2020. 3, 7, 8
- [22] Z. Xie, S. Wang, Q. Yu, X. Tan, and Y. Xie, "Csfwinformer: Cross-space-frequency window transformer for mirror detection," IEEE Trans. on Image Processing, vol. 33, pp. 1853–1867, 2024. 3, 7, 8, 9, 10
- [23] W. Zhou, Y. Cai, L. Zhang, W. Yan, and L. Yu, "Utlnet: Uncertainty-aware transformer localization network for rgb-depth mirror segmentation," IEEE Trans. on Multimedia, vol. 26, pp. 4564–4574, 2023. 4
- [24] T. Yan, X. Zhu, X. Chen, W. He, C. Wang, Y. Yang, Y. Wang, and X. Chang, "Glgfn: Global-local grafting fusion network for high-resolution image deraining," IEEE Trans. on Circuits and Systems for Video Technology, vol. 34, no. 11, pp. 10860–10873, 2024.
- [25] Z. Liu, H. Hu, Y. Lin, Z. Yao, Z. Xie, Y. Wei, J. Ning, Y. Cao, Z. Zhang, L. Dong et al., "Swin transformer v2: Scaling up capacity and resolution," in CVPR, 2022. 4, 7
- [26] S. Xie, R. Girshick, P. Dollár, Z. Tu, and K. He, "Aggregated residual transformations for deep neural networks," in CVPR, 2017. 4
- [27] J. Sun, Y. Chang, C. Jung, and J. Feng, "Multi-modal reflection removal using convolutional neural networks," IEEE Signal Processing Letters, vol. 26, no. 7, pp. 1011–1015, 2019.
- [28] M. Lee, S. Cho, D. Lee, C. Park, J. Lee, and S. Lee, "Guided slot attention for unsupervised video object segmentation," in <u>CVPR</u>, 2024.
- [29] S. Wang, D. Liang, J. Song, Y. Li, and W. Wu, "Dabert: Dual attention enhanced bert for semantic matching," <u>ICCL</u>, 2022.
- [30] P.-T. De Boer, D. P. Kroese, S. Mannor, and R. Y. Rubinstein, "A tutorial on the cross-entropy method," <u>Annals of Operations Research</u>, vol. 134, pp. 19–67, 2005. 7
- [31] X. Qin, Z. Zhang, C. Huang, C. Gao, M. Dehghan, and M. Jagersand, "Basnet: Boundary-aware salient object detection," in CVPR, 2019.
- [32] T. Zhou, H. Fu, G. Chen, Y. Zhou, D.-P. Fan, and L. Shao, "Specificity-preserving rgb-d saliency detection," in ICCV, 2021. 8
- [33] R. Cong, Q. Lin, C. Zhang, C. Li, X. Cao, Q. Huang, and Y. Zhao, "Cirnet: Cross-modality interaction and refinement for rgb-d salient object detection," <u>IEEE Tran. on Image Processing</u>, vol. 31, pp. 6800–6815, 2022. 7, 8
- [34] R. Cong, K. Zhang, C. Zhang, F. Zheng, Y. Zhao, Q. Huang, and S. Kwong, "Does thermal really always matter for rgb-t salient object detection?" <u>IEEE Trans. on Multimedia</u>, vol. 25, pp. 6971–6982, 2022.
 7. 8
- [35] E. Xie, W. Wang, W. Wang, P. Sun, H. Xu, D. Liang, and P. Luo, "Segmenting transparent object in the wild with transformer," in <u>IJCAI</u>, 2021. 3, 9

- [36] J. Zhang, K. Yang, A. Constantinescu, K. Peng, K. Müller, and R. Stiefelhagen, "Trans4trans: Efficient transformer for transparent object segmentation to help visually impaired people navigate in the real world," in ICCV, 2021.
- [37] J. Zhang, K. Yang, A. Constantinescu, K. Peng, K. Müller, and R. Stiefelhagen, "Trans4trans: Efficient transformer for transparent object and semantic scene segmentation in real-world navigation assistance," <u>IEEE Trans. Intell. Transp. Syst.</u>, vol. 23, no. 10, pp. 19173– 19186, 2022. 3
- [38] Y. Zhu, J. Qiu, and B. Ren, "Transfusion: A novel slam method focused on transparent objects," in ICCV, 2021. 3, 7
- [39] Y. Liang, B. Deng, W. Liu, J. Qin, and S. He, "Monocular depth estimation for glass walls with context: a new dataset and method," <u>IEEE Trans. on Pattern Analysis and Machine Intelligence</u>, vol. 45, no. 12, pp. 15 081–15 097, 2023. 3
- [40] A. Kalra, V. Taamazyan, S. K. Rao, K. Venkataraman, R. Raskar, and A. Kadambi, "Deep polarization cues for transparent object segmentation," in CVPR, 2020. 3
- [41] Y. Xu, H. Nagahara, A. Shimada, and R.-i. Taniguchi, "Transcut: Transparent object segmentation from a light-field image," in <u>ICCV</u>, 2015. 3
- [42] X. Yang, H. Mei, K. Xu, X. Wei, B. Yin, and R. W. Lau, "Where is my mirror?" in ICCV, 2019. 3
- [43] T. Huang, B. Dong, J. Lin, X. Liu, R. W. Lau, and W. Zuo, "Symmetry-aware transformer-based mirror detection," in AAAI, 2023. 3
- [44] H. Guan, J. Lin, and R. W. Lau, "Learning semantic associations for mirror detection," in CVPR, 2022. 3
- [45] X. Tan, J. Lin, K. Xu, P. Chen, L. Ma, and R. W. Lau, "Mirror detection with the visual chirality cue," <u>IEEE Trans. on Pattern Analysis and Machine Intelligence</u>, vol. 45, no. 3, pp. 3492–3504, 2022. 3
- [46] Blender, "blender," https://www.blender.org/, 2024. 1
- [47] W. Zhou, F. Sun, Q. Jiang, R. Cong, and J.-N. Hwang, "Wavenet: Wavelet network with knowledge distillation for rgb-t salient object detection," IEEE Trans. on Image Processing, 2023. 8, 9
- [48] I. Loshchilov and F. Hutter, "Decoupled weight decay regularization," in ICLR, 2019. 7
- [49] P. Krähenbühl and V. Koltun, "Efficient inference in fully connected crfs with gaussian edge potentials," in NeurIPS, 2011. 7
- [50] R. Achanta, S. Hemami, F. Estrada, and S. Susstrunk, "Frequency-tuned salient region detection," in CVPR, 2009.
- [51] S. Woo, J. Park, J.-Y. Lee, and I. S. Kweon, "Cbam: Convolutional block attention module," in <u>ECCV</u>, 2018. 9, 11
- [52] J. Deng, W. Dong, R. Socher, L.-J. Li, K. Li, and L. Fei-Fei, "Imagenet: A large-scale hierarchical image database," in CVPR, 2009. 7
- [53] O. Ronneberger, P. Fischer, and T. Brox, "U-net: Convolutional networks for biomedical image segmentation," in MICCAI, 2015. 5
- [54] J. Lin, Y.-H. Yeung, S. Ye, and R. W. Lau, "Leveraging rgb-d data with cross-modal context mining for glass surface detection," in <u>AAAI</u>, 2025. 1, 2, 4, 8
- [55] Z. Shi, Y. Li, and F. Zhang, "Reflection removal via recurrent learning guided by physics prior and focal perceptual loss," <u>IEEE Trans. on Circuits and Systems for Video Technology</u>, vol. 34, no. 10, pp. 10152– 10165, 2024. 2
- [56] B. Jiang, Y. Lu, B. Zhang, and G. Lu, "Few-shot learning for image denoising," <u>IEEE Trans. on Circuits and Systems for Video Technology</u>, vol. 33, no. 9, pp. 4741–4753, 2023.
- [57] M. Zha, F. Fu, Y. Pei, G. Wang, T. Li, X. Tang, Y. Yang, and H. Tao Shen, "Dual domain perception and progressive refinement for mirror detection," <u>IEEE Trans. on Circuits and Systems for Video</u> <u>Technology</u>, vol. 34, no. 11, pp. 11942–11953, 2024. 3
- [58] H. Gao, F. Wang, M. Wang, F. Sun, and H. Li, "Highly efficient rgb-d salient object detection with adaptive fusion and attention regulation," <u>IEEE Trans. on Circuits and Systems for Video Technology</u>, pp. 1–1, 2024. 4, 7, 8
- [59] W. Zhou, B. Jian, M. Fang, X. Dong, Y. Liu, and Q. Jiang, "Dgpinet-kd: Deep guided and progressive integration network with knowledge distillation for rgb-d indoor scene analysis," <u>IEEE Trans. on Circuits and Systems for Video Technology</u>, vol. 34, no. 9, pp. 7844–7855, 2024. 4
- [60] G. Li, Y. Wang, Z. Liu, X. Zhang, and D. Zeng, "Rgb-t semantic segmentation with location, activation, and sharpening," <u>IEEE Trans. on</u> <u>Circuits and Systems for Video Technology</u>, vol. 33, no. 3, pp. 1223– 1235, 2023. 4, 7, 8
- [61] S. Yao, M. Zhang, Y. Piao, C. Qiu, and H. Lu, "Depth injection framework for rgbd salient object detection," <u>IEEE Trans. on Image</u> Processing, vol. 32, pp. 5340–5352, 2023. 4

- [62] G. Feng, J. Meng, L. Zhang, and H. Lu, "Encoder deep interleaved network with multi-scale aggregation for rgb-d salient object detection," Pattern Recognition, vol. 128, p. 108666, 2022. 4
- [63] J. He, Y. Wang, L. Wang, H. Lu, B. Luo, J.-Y. He, J.-P. Lan, Y. Geng, and X. Xie, "Towards deeply unified depth-aware panoptic segmentation with bi-directional guidance learning," in ICCV, 2023. 4
- [64] F. Wang, Y. Su, R. Wang, J. Sun, F. Sun, and H. Li, "Cross-modal and cross-level attention interaction network for salient object detection," <u>IEEE Trans. on Artificial Intelligence</u>, vol. 5, no. 6, pp. 2907–2920, 2024 4
- [65] Q. Chang, H. Liao, X. Meng, S. Xu, and Y. Cui, "Panoglassnet: Glass detection with panoramic rgb and intensity images," <u>IEEE Trans. on Instrumentation and Measurement</u>, vol. 73, pp. 1–15, 2024.
- [66] T. Zhou, H. Fu, G. Chen, Y. Zhou, D. Fan, and L. Shao, "Specificity-preserving RGB-D saliency detection," in ICCV, 2021.
- [67] S. He and R. W. Lau, "Saliency detection with flash and no-flash image pairs," in ECCV, 2014, pp. 110–124.
- [68] Z. Xia, M. Gharbi, F. Perazzi, K. Sunkavalli, and A. Chakrabarti, "Deep denoising of flash and no-flash pairs for photography in low-light environments," in CVPR, 2021, pp. 2063–2072.
- [69] J. Xu, X. Deng, C. Zhang, S. Li, and M. Xu, "Laplacian gradient consistency prior for flash guided non-flash image denoising," <u>IEEE</u> <u>Trans. on Image Processing</u>, 2024. 3
- [70] G. Petschnigg, R. Szeliski, M. Agrawala, M. Cohen, H. Hoppe, and K. Toyama, "Digital photography with flash and no-flash image pairs," ACM trans. on graphics (TOG), vol. 23, no. 3, pp. 664–672, 2004.
- [71] X. Cao, M. Waechter, B. Shi, Y. Gao, B. Zheng, and Y. Matsushita, "Stereoscopic flash and no-flash photography for shape and albedo recovery," in CVPR, 2020, pp. 3430–3439.
- [72] Y. Chang, C. Jung, J. Sun, and F. Wang, "Siamese dense network for reflection removal with flash and no-flash image pairs," <u>International</u> Journal of Computer Vision, vol. 128, no. 6, pp. 1673–1698, 2020. 3
- [73] S. S. Maralan, C. Careaga, and Y. Aksoy, "Computational flash photography through intrinsics," in CVPR, 2023, pp. 16654–16662.
- [74] K. Fan, C. Wang, Y. Wang, C. Wang, R. Yi, and L. Ma, "Rfenet: Towards reciprocal feature evolution for glass segmentation," in <u>IJCAI</u>, 2023.